Doctoral Dissertation (Censored)

博士論文 (要約)

Spectroscopy of resonance states in light proton-rich nuclei via missing mass method

(欠損質量法を用いた軽い陽子過剰核における共鳴状態の分光)

A Dissertation Submitted for the Degree of Doctor of Philosophy
December 2019

令和元年12月博士(理学)申請

Department of Physics, Graduate School of Science,

The University of Tokyo

東京大学大学院理学系研究科物理学専攻

Shumpei Koyama

小山　俊平

Abstract

In this study, excited states of unstable ^{8}C nucleus, the most proton-rich even-even nuclei ever observed, were experimentally investigated. Experimental observables of light proton-rich nuclei are still limited and imporant as a basis of the study. The observables are essential to understand the specific correlations such as the cluster structure which are expected to appear in light nuclei, expecially in unstable nuclei and excited states in stable nuclei.

We performed the experiment to measure excited state of ^{8}C by using the missing mass method at the accelerator facility GANIL. Resonance states in ^{8}C were populated via the (p, d) and (p, t) reactions with 55 MeV/u ^{9}C and ^{10}C secondary beams and a liquid hydrogen target. Resonance states in ^{7}B, ^{6}Be and ^{5}Li were also measured via the (p, d) reaction in the same setup.

We successfully obtained the excitation energy spectra of ^{8}C. The first 2^{+} state of ^{8}C was newly observed at 3.4(2) MeV with the broad decay width of 3.0(4) MeV. For the 2^{+} state of ^{8}C, the excitation energy was compared with that of the mirror nuclei ^{8}He. The moderate value of the mirror energy difference suggests the mirror symmetry is preserved in the 2^{+} states with the broad decay width of ^{8}C.

In addition to the first excited state of ^{8}C, the resonances around 17 MeV in the $N = 2$ isotones were observed systematically. These resonances are understood as the deep s hole states as previously observed in ^{5}Li.

Contents

Chapter 1

Introduction

1.1 Structure of light nuclei

An atomic nucleus discovered in 1911 [1] is a finite quantum many-body system consisting of protons and neutrons, namely nucleons. Nucleons in a nucleus interact with each other by the nuclear force as well as the repulsive Coulomb force for each proton pairs. Nuclei are characterized by the number of protons Z and that of neutrons N. The structures of nuclei and the reactions with nuclei have been investigated for more than one hundred years.

Large variety of observables of nuclei such as masses, excited states, spin-parities of states have been experimentally measured in many nuclei. In order to theoretically describe these observables systematically, the nuclear system have been modeled to reduce the number of degree of freedom since it was difficult to directly treat a nucleus as a many-body system even with several nucleons. The binding energy of a nucleus was generally explained by the Bethe-Weizsäcker formula based on the liquid drop model in 1935 [2]. In a large mass region, nuclear structures have been well described by the shell model based on the independent particle model, in which a single nucleon moves in a mean field potential including the spin-orbit interaction in 1949 [3, 4].

In light nuclei, especially in unstable nuclei and excited states in stable nuclei, some specific correlations such as α-cluster [5, 6], halo [7] and di-neutron correlations have been suggested. A state with the α-cluster structure in ^{12}C was predicted in 1954 by Hoyle [8] and the corresponding state known as Hoyle state was experimentally observed soon after as the 0^+ excited state at 7.65 MeV [9]. The two-neutron halo structure was firstly claimed in the ground state of neutron-rich ^{11}Li from the measurement of the large matter radius [10] and the narrow momentum distribution [11] in 1980s. The di-neutron correlation, spatially localized two neutrons in a nucleus [12], was further suggested in the

ground state of ^{11}Li [13]. Many models such as the cluster model have been developed to describe these correlations.

For the straight-forward descriptions of nuclear structures without any model, significant progress of *ab initio* calculations has been made in recent years [14]. *Ab initio* calculations in nuclear physics start from the fundamental forces among nucleons and aim at predicting the properties of nuclei. The non-relativistic many-nucleon Schrödinger equation is solved with the inter-nucleon interactions as the only input. The equation can be solved exactly for the lightest nuclei up to $A = 4$ [15]. The calculations have become applicable to the description of bound-state properties of light and medium mass nuclei by using many methods, such as the Green's function Monte Carlo method [16], the coupled clusters method [17] and the no-core shell model [18].

As a result of *ab initio* calculations, the specific correlations in light nuclei as mentioned above, which was predicted but difficult to directly observe in experiments, have appeared. For example, the calculation of ^{8}Be with the Green's function Monte Carlo method exhibited the cluster structure composed of two α particles [19]. *Ab initio* calculations are expected to shed light on the mechanism of the several correlations by directly comparing experimental observables with theoretical calculations.

As a basis of the study, it is essential to accumulate experimental observables of light nuclei, especially in unstable nuclei and excited states in stable nuclei, in which specific correlations are expected to appear. Experimental results in light unstable nuclei are still not complete though the development of radioactive isotope (RI) beams allow to investigate unstable nuclei effectively. Experimental results of proton-rich nuclei are more limited than those of neutron-rich nuclei. This is because the proton-rich nuclei are less particle-bound with larger repulsive Coulomb force and difficult to access experimentally.

In the present study, excited states of ^{8}C are experimentally investigated. ^{8}C is composed of six protons and two neutrons, the most proton-rich even-even nuclei ever observed. Only the ground state of ^{8}C was experimentally observed in several experiments [20, 21, 22, 23, 24, 25]. The ground state is a resonance state, which is particle unbound relative to the four proton emission threshold of -3.48 MeV. The total decay width of the ground state was measured to be 130(50) keV [24].

While no excited state has been reported in ^{8}C, the first excited state of ^{8}C can be predicted to exist from the mirror symmetry of nuclei. The mirror symmetry is one of the basic features in the nuclear system. The mirror nuclei are defined as a pair of nuclei with interchanged numbers of protons and neutrons. The level schemes of the mirror nuclei are known to be almost the same. As an example, the low-lying level schemes of the mirror nuclei ^{11}C and ^{11}B are shown in Fig. 1.1. Excited states with the same spin-parity appear at almost the same excitation energies. This indicates that the structures

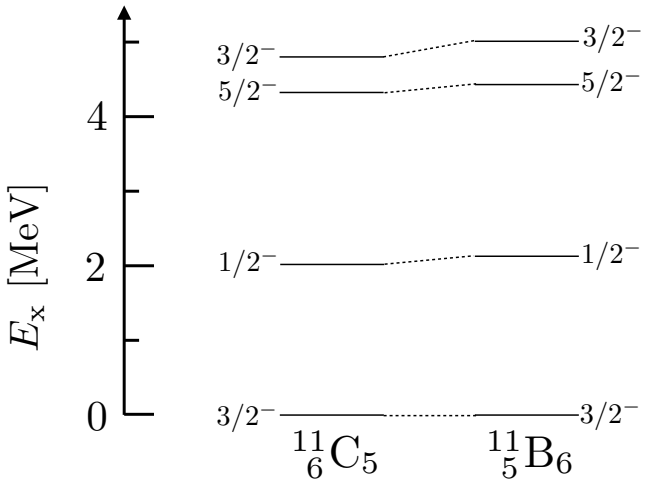

Fig. 1.1 Low-lying level schemes of a pair of mirror nuclei ^{11}C and ^{11}B up to 6 MeV.

of the ground and excited states of mirror nuclei are the same except for the effect of the Coulomb force. The first excited 2^+ state of ^{8}He, which is the mirror nucleus of ^{8}C, was experimentally reported as a resonance in several experiments [26, 27, 28, 29, 30]. In these experiments, the excitation energy of the 2^+ state was reported from 3.5 to 3.6 MeV while the width of that was 0.5 to 1.0 MeV. The excitation energy of 3.53(4) and the decay width of 0.89(11) MeV [30] are used as a reference in this thesis with the smallest error bar among the previous experiments. The spin-parity of this state was assigned by the angular distribution of the proton inelastic scattering [26, 30]. Therefore, the first 2^+ state of ^{8}C is expected to appear around the excitation energy of 3.5 MeV.

The low-lying level schemes of ^{8}C and ^{8}He are shown in Fig. 1.2. The level schemes of neighboring even-even nuclei ^{6}Be and ^{6}He are also shown as a reference. Few excited states are expected in these nuclei since the number of the nucleon is small. In fact, only the first 2^+ states have been observed in ^{6}Be and ^{6}He up to an excitation energy of 10 MeV. The total decay width of the 2^+ state in proton-rich ^{6}Be is about ten times larger than that in neutron-rich ^{6}He. The 2^+ state of proton-rich ^{8}C is expected to have a large decay width because even the width of the mirror state in neutron-rich ^{8}He is 0.89(11) MeV. In nuclear system, the decay width of a resonance state takes a wide range of value from a few eV to several MeV, about 10^6 times difference. For example, the decay width of the ground 0^+ state of ^{8}Be is 5.57 eV while that of the excited 4^+ state of ^{8}Be is 3.5 MeV [31]. The life time of a resonance state is inversely proportional to the decay width as

$$\tau = \frac{\hbar}{\Gamma}. \tag{1.1}$$

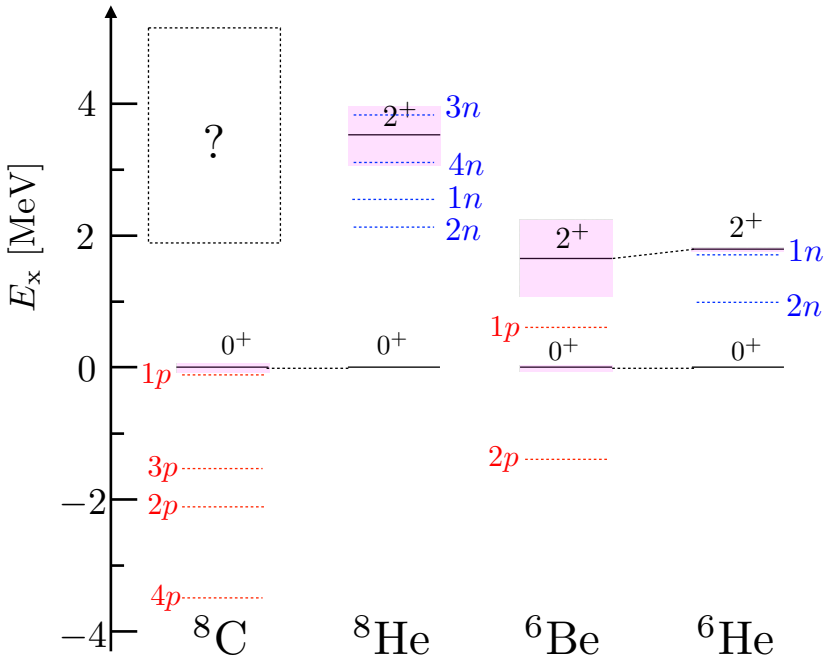

Fig. 1.2 Low-lying level schemes of ^{8}C, ^{8}He, ^{6}Be and ^{6}He. The total decay width of the resonance states are shown by magenta band. The threshold energies of proton emission is shown by red dotted line while those of neutron emission by blue dotted line.

A typical decay width of 1 MeV corresponds to 7×10^{-22} s. The typical time scale of nuclei is also calculated as the necessary time of a neucleon with the Fermi energy passing through a diameter of a nucleus. This time is about 6×10^{-23} s with the the Fermi energy of 40 MeV and a typical diameter of 5 fm [32]. The life time and the typical time scale will be the same order of magnitude when the decay width is more than a few MeV. It is not obvious that the structure of a resonance state with a broad decay width, which is predicted for the first excited state of ^{8}C, is well established with such a short life time.

In terms of theoretical calculations, no excited states in ^{8}C have been calculated. In light nuclei, *ab initio* calculations of resonance properties are under development with such as the no-core shell model with resonating-group method [33] and the coupled clusters method with the Gamow basis [34]. The resonance states of ^{5}He was calculated as a five-body problem and compared with the experimental data of two-body neutron and ^{4}He scattering [35]. The bound and resonance states of ^{6}He was also calculated as a six-body problem to study the three-body resonance property of two neutrons and ^{4}He [36]. These calculations are expected to develop to more than three-body resonance, such as five-body resonance in ^{4}He and four nucleons in ^{8}C and ^{8}He in the near future. The experimental observable in ^{8}C will help to verify the calculations of many-body resonance.

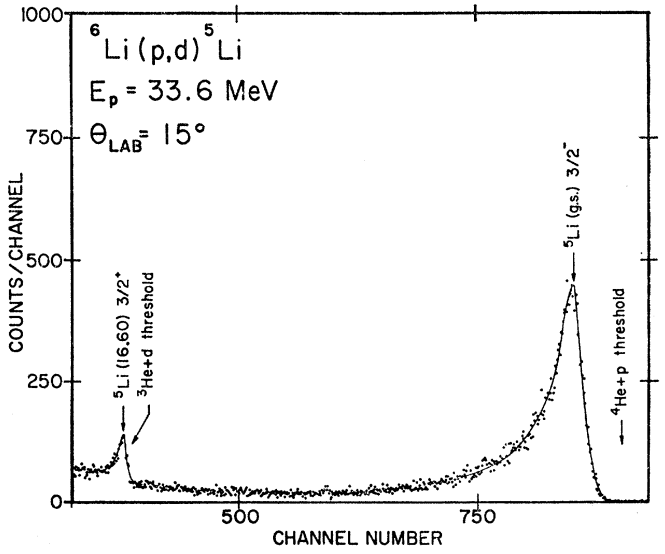

Fig. 1.3 Deuteron spectrum from the ^{6}Li$(p,d)^5$Li reaction. Two peaks were observed. The figure is taken from Ref. [37].

1.2 Reaction

In order to investigate excited states in ^{8}C experimentally, the one-neutron transfer reaction is effective. Particle unbound states in ^{8}C are populated by removing a neutron from the particle-bound ground state of ^{9}C. Only the states with protons and neutrons in $1s$ and $1p$ orbits are expected to be populated while the excited states in the higher orbits such as the next sd orbit are expected to be suppressed. For the one-neutron transfer transfer reaction, the (p,d) reaction is often utilized with the relatively simple reaction mechanism [38].

The spectrum of the ^{9}C$(p,d)^8$C reaction can be estimated by the experimental result of the ^{6}Li$(p,d)^5$Li reaction, where ^{5}Li is one of the isotones of ^{8}C. The experimental result of the ^{6}Li$(p,d)^5$Li reaction is shown in Fig. 1.3 [37]. Two peaks were clearly observed, one was the ground $3/2^-$ state of ^{5}Li and the other was the excited $3/2^+$ state at 16.87 MeV. This experimental observation can be simply understood by the single-particle configuration. The possible single-particle configuration of the ^{6}Li$(p,d)^5$Li reaction is shown in Fig. 1.4. The ground state of ^{6}Li is understood as the full occupancy in $s_{1/2}$ and one proton and neutron in $p_{3/2}$. When a neutron in $p_{3/2}$ is removed, the $3/2^-$ ground state of ^{5}Li is populated. On the other hand, when a deeply bound neutron in $s_{1/2}$ is removed, the highly excited state of ^{5}Li at 16.87 MeV is populated.

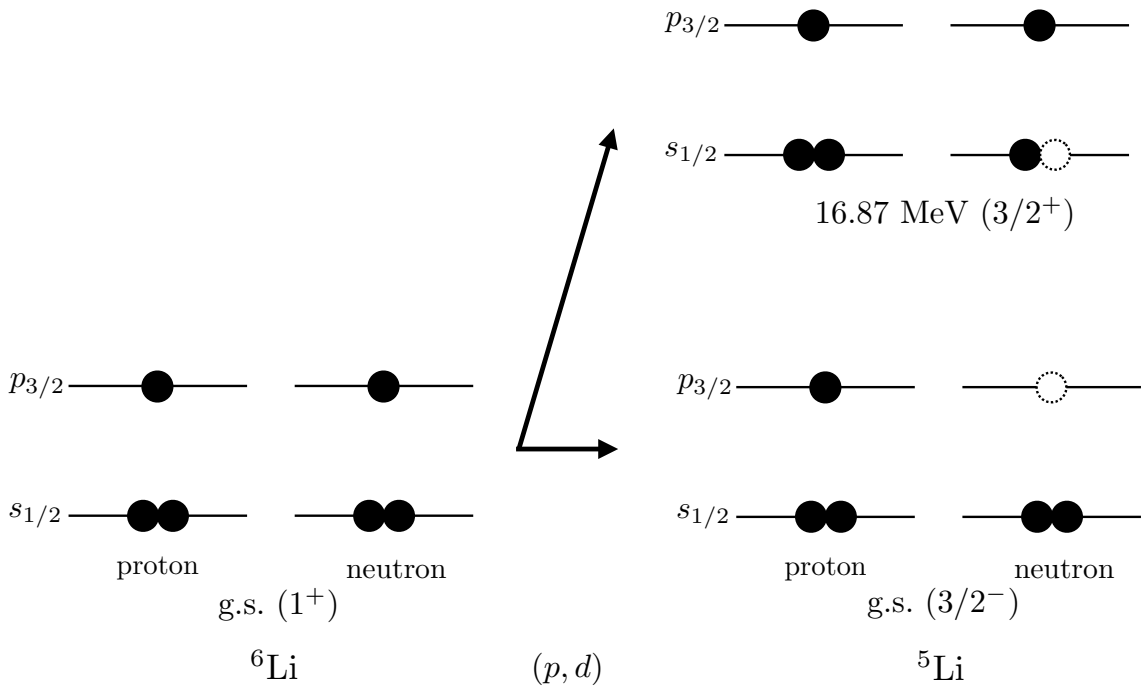

Fig. 1.4 Possible single-particle configuration for the ^{6}Li$(p, d)^5$Li reaction.

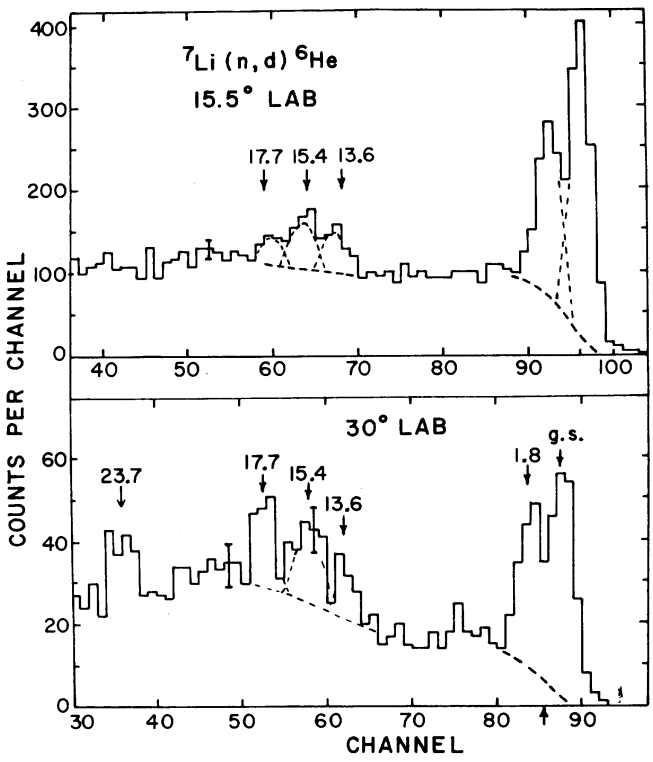

Fig. 1.5 Deuteron spectrum from the ^{7}Li$(n, d)^6$He reaction. Two groups of peaks were observed. The figure is taken from Ref. [39].

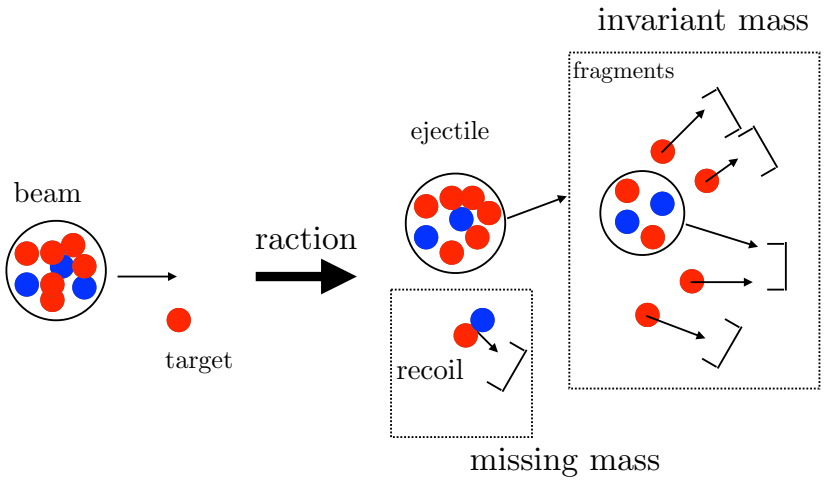

Fig. 1.6 Schematic drawing of two experimental methods.

This simple explanation can also be applied to the one-proton transfer (n, d) reaction with ^{7}Li. The experimental result of the $^{7}\mathrm{Li}(n, d)^{6}\mathrm{He}$ reaction is shown in Fig. 1.5 [39], which is similar to that of the $^{6}\mathrm{Li}(p, d)^{5}\mathrm{Li}$. In the case of the $^{7}\mathrm{Li}(n, d)^{6}\mathrm{He}$ reaction, the ground state and first excited 2^{+} state at 1.8 MeV of ^{6}He were populated by removing a proton in p orbit. Highly excited states around 15 MeV were also populated by removing a proton in s orbit.

This simple explanation is, however, not applied to heavier nuclei especially for the neucleon transfer from deeply bound s orbit. The strength of the deep hole s state have been clearly observed in light nuclei but not in heavier nuclei by the systematic study of proton knock-out reaction, which has a similar selectivity as the transfer reaction [40]. In heavier nuclei, the deep hole s state produced by a one-nucleon transfer reaction propagate in a compound state by coupling with many-particle-many-hole states [41]. This is because the deep hole state appears in a high excitation energy region and the level density is very high in such an energy region. As a result, the main component of a deep hole state in heavier nuclei is fragmented statistically. In light nuclei, the small number of the possible configurations prevent the deep hole state from being fragmented.

As with the results of the $^{6}\mathrm{Li}(p, d)^{5}\mathrm{Li}$ and $^{7}\mathrm{Li}(n, d)^{6}\mathrm{He}$ reactions, the first excited state of ^{8}C is expected to be populated by the $^{9}\mathrm{C}(p, d)^{8}\mathrm{C}$ reaction by removing a neutron in p orbit. In addition to the lower-lying state, a deep s hole state in ^{8}C may be populated.

1.3 Experimental method

For the spectroscopy of resonance states with RI beams by the inverse kinematics, two methods are used. One is the missing mass method and the other is the invariant mass method. A schematic drawing of two experimental methods is shown in Fig. 1.6. By the missing mass method, the four momentum of the recoil particle from the target is measured to reconstruct the excitation energy. The advantage of this method is that it requires only single-particle detection without detecting the decay fragments from a resonance state. The angular distribution, which is useful to determine the spin-parity of the state, can be easily obtained. However, the resolution of the excitation energy spectrum by the missing mass method is worse than that by the invariant method. This is due to the low kinetic energy of the recoil particle from the fixed target. Even a small amount of the energy loss of the recoil particle in the target affects the resolution of the excitation energy. By the invariant mass method, the four momenta of the beam-like fragments are measured to reconstruct the excitation energy. The kinetic energies of the fragments hardly affect by the energy loss in the target since the beam-like fragments have almost the same kinetic energy per nucleon as the RI beam. As a consequence, the resolution of the excitation energy is reasonable. The detailed decay scheme of the resonance state can be also investigated. However, it is difficult to measure all the four momenta of the decay fragments when the number of emitted particles is large due to the geometrical acceptance for multiple particles.

In the present study, the missing mass method was used with proton-rich RI beams with the kinetic energy of 55 MeV/u. In addition to the ^{9}C$(p,d)^{8}$C reaction, the ^{10}C$(p,t)^{8}$C reaction was also measured with a ^{10}C beam. The resonance states of ^{8}C are expected to decay via five-particle, an α particle and four protons, emission. The single-particle detection by the missing mass is more efficient than the multi-particle detection by the invariant mass method. The low kinetic energy of the recoil particle with the missing mass method, is solved by a specific reaction as explained later.

The practical advantage of the (p,d) and (p,t) reactions is relatively high kinetic energy of the recoil particle from the target. The reactions utilized in the present study requires large negative Q-values. In the case of the ^{9}C$(p,d)^{8}$C and ^{10}C$(p,t)^{8}$C reactions, the Q-values are -12 MeV and -27 MeV, respectively. The large negative Q-value reduces the energy of the ejectile particle relative to the kinetic energy of the beam particle. The recoil particle gains the kinetic energy in the laboratory frame for the momentum conservation. The kinetic energies of the recoil deuteron and triton leading to the ground state of ^{8}C are more than 16 and 55 MeV, respectively. The large kinetic energy allow to use a thick

hydrogen target without losing the energy resolution of the excitation energy spectra by the missing mass method. High luminosity is realized by using a thick hydrogen target. In the present experiment, a liquid hydrogen target with a thickness of 1.5 mm at the center.

The experiment with the same method was performed to investigate the structure of proton-rich oxygen isotopes [42, 43, 44]. The low-lying states in ^{12}O and ^{13}O were successfully observed with relatively high statistics and reasonable resolution. The $^{10}\mathrm{C}(p,t)^{8}\mathrm{C}$ reaction was once measured [25]. Only the ground state of ^{8}C was observed. Note that only the most forward angle was measured in Ref. [25].

In the ^{9}C beam produced by the fragmentation reaction, the $N = 3$ isotones ^{8}B, ^{7}Be and ^{6}Li are inevitably included as described in Sect. 2.2.1. Therefore, the $^{9}\mathrm{C}(p,d)^{8}\mathrm{C}$, $^{8}\mathrm{B}(p,d)^{7}\mathrm{B}$, $^{7}\mathrm{Be}(p,d)^{6}\mathrm{Be}$ and $^{6}\mathrm{Li}(p,d)^{5}\mathrm{Li}$ reactions can be measured simultaneously in one setup. For the $^{8}\mathrm{B}(p,d)^{7}\mathrm{B}$ and $^{7}\mathrm{Be}(p,d)^{6}\mathrm{Be}$ reactions, highly excited states in ^{7}B and ^{6}Be, which have not been reported, may be populated by removing a deeply bound neutron in $s_{1/2}$ as in the case of the $^{6}\mathrm{Li}(p,d)^{5}\mathrm{Li}$ reaction.

1.4 Thesis objective

In this thesis, we present an experimental research of the excited state of ^{8}C. We performed an missing mass experiment of the (p,d) and (p,t) reactions to populate particle-unbound excited states of ^{8}C with RI beams and a liquid hydrogen target. The deep s hole states in $N = 2$ isotones were simultaneously measured in the same setup.

The author took a major role throughout the experiment. Especially, he took the responsibility of the liquid hydrogen for the preparation and operation during the main experiment. The configuration of the light particle telescopes were optimized to measure both of the (p,d) and (p,t) reactions in one setup by him. The entire part of the data analysis was performed by him.

This thesis is organized as follows. First, the performed experiment is explained in Chap. 2. Next, we present the data analysis to obtain an excitation energy spectra of the (p,d) and (p,t) reactions in Chap. 3. The experimental results are summarized in Chap. 4. The structures of the newly observed resonance states are discussed in Chap. 5. Finally, conclusion and future outlook are given in Chap. 6.

Chapter 2

Experiment

In this chapter, we describe the details of the experiment.

2.1 Accelerator facility

The present experiment was carried out as the E738 experiment in July 2018 at the accelerator facility, Grand Accélérateur National d'Ions Lourds (GANIL) in Caen, France. We performed the E738 experiment following the E755 experiment, in which different beams and the same setup were used. The layout of the experimental facility GANIL is shown in Fig. 2.1. A wide range of ions can be accelerated with several beam energy up to 95 MeV/u by the combination of five cycrotorons as a primary beam.

Two methods for RI beam production are available at GANIL. One is the in-flight projectile fragmentation method by the Ligne d'Ions Super Epluchés (LISE) spectrometer or by the ALPHA spectrometer. RI beams with several tens of MeV/u kinetic energy are produced by these spectrometers. The other is the Isotope Separator On-Line (ISOL) method by the SPIRAL1 beam line. RI beams with from a few keV to 20 MeV/u kinetic energy are produced. The primary beam itself or the RI beam is extracted and transferred to experimental areas such as G1 with the VAriable MOde Spectrometer (VAMOS) spectrometer, D5 with Identification de Noyaux et Détection avec Résolutions Accrues (INDRA) and so on. Many varieties of experiments can be performed with the combination of the beams and the experimental devices.

In the present experiment, a 75 MeV/u ^{12}C beam accelerated by CSS1 and CSS2 was used as the primary beam. The typical beam intensity was 1.8 eμA. The radio frequency (RF) of the acceleration was 13 MHz. This corresponds to 76-ns bunch interval. The beam was transported to the LISE spectrometer and the RI beams were produced by the in-flight projectile fragmentation method.

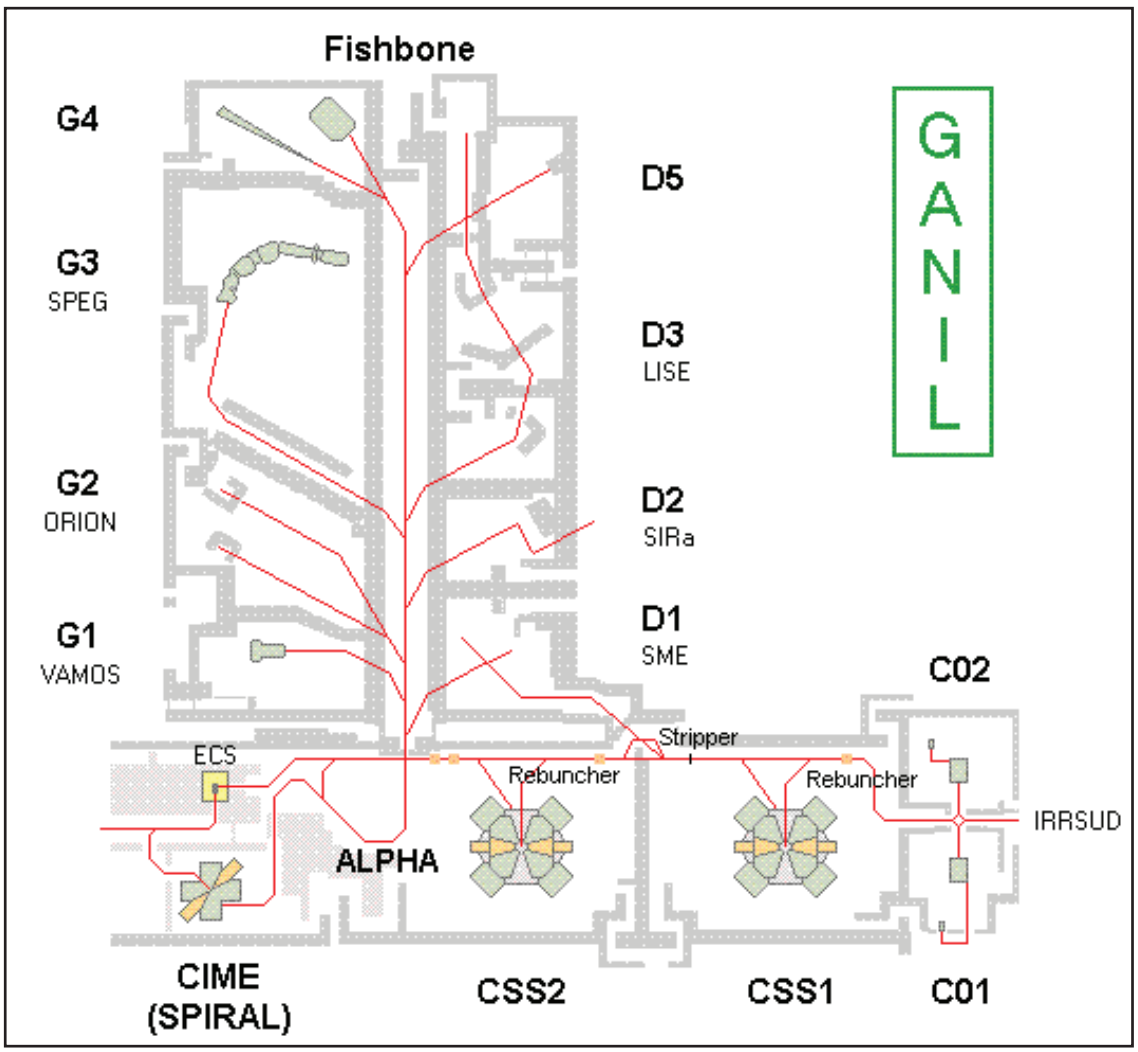

Fig. 2.1 A schematic layout of the GANIL facility.

2.2 Secondary beam line

The RI beams was produced by the projectile fragmentation reaction of a stable ^{12}C primary beam. Two secondary beams, the ^{9}C beam and the ^{10}C beam, were produced by the LISE fragment separator. The production method and the detail of the beam line of the LISE spectrometer is described in this section.

2.2.1 Projectile fragment separator LISE

The primary beam with an energy of 75 MeV/u impinged onto a ^{9}Be production target with a thickness of 2.156 mm. By the projectile fragmentation reaction, a cocktail of

secondary beam particles with several masses and different A/Z ratios were produced. To collect the produced particles and separate the isotopes of interest, the LISE spectrometer was used as a projectile fragment separator.

Figure 2.2 shows the schematic view of the LISE spectrometer [45, 46]. The LISE spectrometer consists of 4 dipole magnets and 25 quadrapole magnets. The separator has the momentum acceptance of $\Delta p/p = \pm 2.5$ % and the angular acceptance of $\Delta\Omega = 1$ msr. A detector, CAVIAR, was placed in the middle of the beam line, which was not used in the present analysis. The detail of the detector is mentioned in Appx. A.

The particle separation was performed by the $B\rho - \Delta E - B\rho$ method [45]. By the selection of magnetic rigidity between the production target and the first dispersive focal plane, the $A/Z \times v$ values of the particles are chosen. The velocity v from the projectile fragmentation reactions are almost constant. Therefore the first selection corresponds to the selection of A/Z values. This selection is achieved with slits in the downstream of the dispersive focal plane, restricting the range of the magnetic rigidity $B\rho$ for the beam to pass. For the further separation, the secondary beam passed through a Be wedge degrader placed on the first dispersive focal plane. By the collision with the atomic electrons in this degrader, the beam particles lose a part of their energy (ΔE) according to the Bethe-Bloch formula. Note that the degrader was wedge shaped to conserve the momentum dispersive condition at the downstream. This means after the first $B\rho$ selection, the momentum of the same kind of a secondary beam particle has some spread. If we use flat degrader, this spread will be wider and the focus after the second $B\rho$ selection will be destroyed. With the appropriate shape of wedge degrader, this focus will be conserved. It is known that the second selection separated according to $A^{2.5}/Z^{1.5}$ value. The values of $A^{2.5}/Z^{1.5}$ are shown in Fig. 2.3

In addition to the common secondary beam production method for the LISE spectrometer, the other selection with Wien filter was performed in the present experiment . In the Wien filter, the electric field is in the vertical and the magnetic field in the horizontal direction to select the velocity. Combining to these three selections, we can obtain purified the RI beams of interest. This selection mode is so-called LISE3.

Though this is a general procedure of the in-flight projectile fragmentation reaction, additional consideration is necessary to produce the secondary beams with proton-rich nuclei. The production rates by the in-flight projectile fragmentation reaction of nuclei with more different A/Z value than that of the stable primary beam nuclei is low. Stable nuclei has the A/Z value close to 2 or a little more. Therefore, the production rate of nucleus with smaller A/Z value, which is more proton-rich nuclei is low. From the first selection, strictly speaking, the selection is not A/Z but $A/Z \times v$. As mentioned above, most of the v of the secondary beam particle is almost the same value of the primary beam,

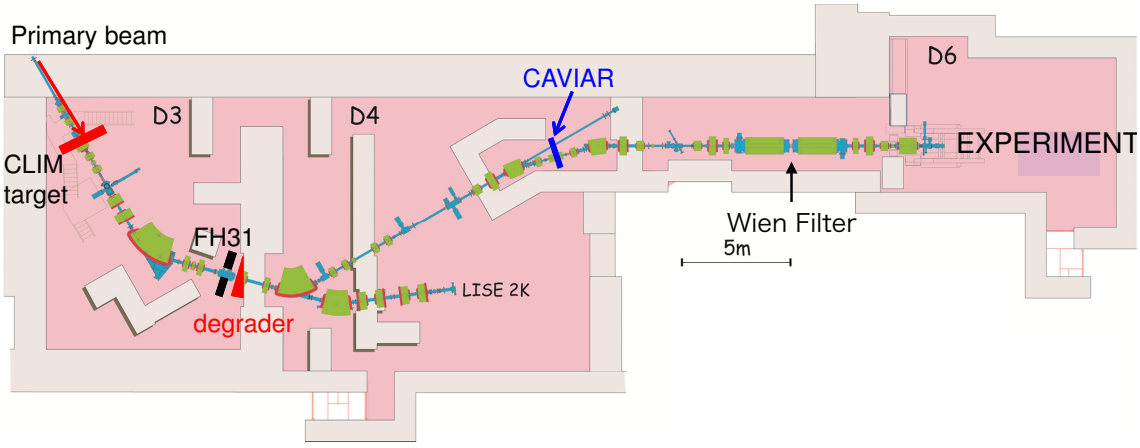

Fig. 2.2 A schematic layout of the LISE spectrometer.

but it can be lower. As a consequence, nuclei with the same $A/Z \times v$ but less proton-rich, which means higher production rate than that of more proton-rich nuclei, can be generated more than the objective particle. As a result, nuclei with close $A^{2.5}/Z^{1.5}$ values of the objective RI will contaminate in the secondary beam from the second selection. On the other hand, more neutron-rich nuclei has larger values of A/Z and v has a maximum value, the v of the primary beam. Therefore such a consideration is not necessary for neutron-rich nuclei.

In the present experiment, the $N = 3$ isotones ^{8}B, ^{7}Be and ^{6}Li were contaminants in the ^{9}C secondary because of similar values of $A^{2.5}/Z^{1.5} \simeq 16.5$. On the other hand the ^{10}C secondary beam was almost pure because the value of $A^{2.5}/Z^{1.5}$ of ^{10}C is equal to about 21.5 and no other nuclei has close value. This is because ^{9}B and ^{8}Be, the isotpne of ^{10}C, are unbound though they have the value of $A^{2.5}/Z^{1.5}$ close to 21.5. In the present case, ^{8}B and ^{7}Be are also RI and they can provide new data. The reaction with ^{6}Li is well known from normal kinematics experiments and will be a reference data. This also means the systematic study for nuclei with the same N can be possible for one secondary beam setting.

The parameters of the secondary beams are shown in Table 2.1. Note that the Magnetic rigidity of D1 for ^{12}C beam setting was higher to transport not fully-stripped ^{12}C but $^{12}C^{5+}$ to reduce the total intensity of the beam. The almost all of $^{12}C^{5+}$ nuclei were fully-stripped at the degrader and transported to downstream.

2.2.2 Reaction chamber

A vacuum chamber named M2C chamber with 1.1-m diameter and 1-m hight was placed as a reaction chamber at the last focus of the LISE beam line, D6 experimental area. The

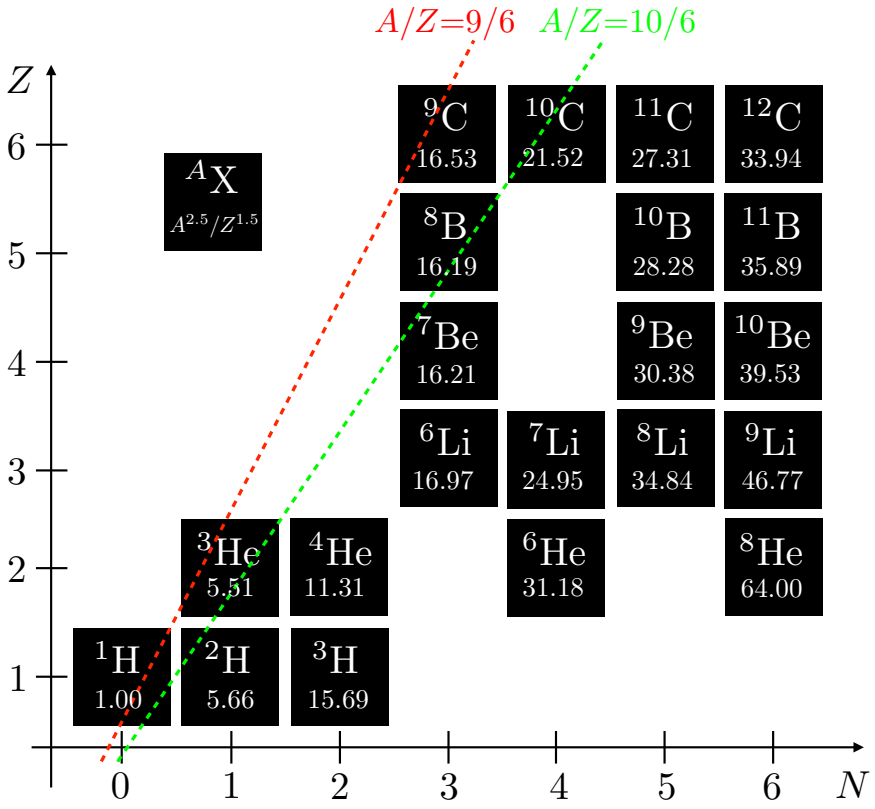

Fig. 2.3 A chart of nuclide. The values of $A^{2.5}/Z^{1.5}$ are shown with nuclide. Only the bound nuclei are shown.

reaction target and the recoil particle detectors with many cables were placed inside the chamber. The zero degree detection system was also placed at the downstream side of the chamber. The beam tracking detectors were placed upstream of the chamber and the vacuum of inside the M2C chamber was disconnected to the vacuum at the upstream. In this chamber, a reaction target and detectors, which will be explained in the following sections, were placed. We will call this "experimental station" hereafter.

For the present experiment, higher level of vacuum in the chamber than usual was required to use cryogenic hydrogen target. For that purpose, three turbo molecular pumps were placed on the top flange of the chamber and a cryopump was placed on the side flange of the chamber. The vacuum level during the experiment was 2×10^{-6} mbar.

2.3 Reaction Target

本節については、5 年以内に雑誌等で刊行予定のため、非公開。

Table 2.1 Parameters of the LISE spectrometer.

	^{9}C	^{10}C	^{12}C
Primary target (Be) thickness [μm]	2156	2156	2156
Degrader (Be) thickness [μm]	1045	1045	2180
Magnetic rigidity D1 [Tm]	1.7301	1.9298	2.8422
Magnetic rigidity D2 [Tm]	1.6352	1.8345	2.1679
Magnetic rigidity DA1 [Tm]	1.6301	1.8288	2.1614
Magnetic rigidity DA2 [Tm]	1.6555	1.8556	2.1907
Slit F31 [mm]	$\pm$20	$\pm$5	$\pm$2
Slit F43 Horizontal [mm]	$\pm$10	$\pm$10	$\pm$10
Slit F43 Vertical [mm]	$\pm$10	$\pm$30	$\pm$10
Slit F62 Horizontal [mm]	$\pm$15	$\pm$15	$\pm$15
Slit F62 Vertical [mm]	$\pm$25	$\pm$20	$\pm$20
Wien filter [kV]	2.5	0	0

2.4 Detection system at the experimental station

2.4.1 Setup

The schematic setup seen from top at the experimental station is shown in Fig. 2.4. The beam tracking detector CATS1 and CATS2 were placed at the upstream of the liquid hydrogen target. TOF relative to RF signal was also measured by CATS1 and CATS2. Target recoil particles from transfer reactions were detected by 8 MUST2 telescopes named T1-T8 placed just downstream of the liquid hydrogen target. Beam-like fragments such as protons and alpha particles were also detected by MUST2. At the downstream of MUST2, the detection system so-called zero degree detectors were placed to detect the beam-like heavy fragments. This was composed of an ionizing chamber, drift chambers and a plastic scintillator.

2.4.2 Secondary beam particle detector; CATS

The beam particle tracking detection is required for the measurements via the missing mass spectroscopy. because the methods of producing radioactive beams lead to larger emittance than for stable ion beams. Typical size of the beam is greater than 1 cm in diameter. Two CATS [48] detectors were installed at just upstream of the M2C chamber

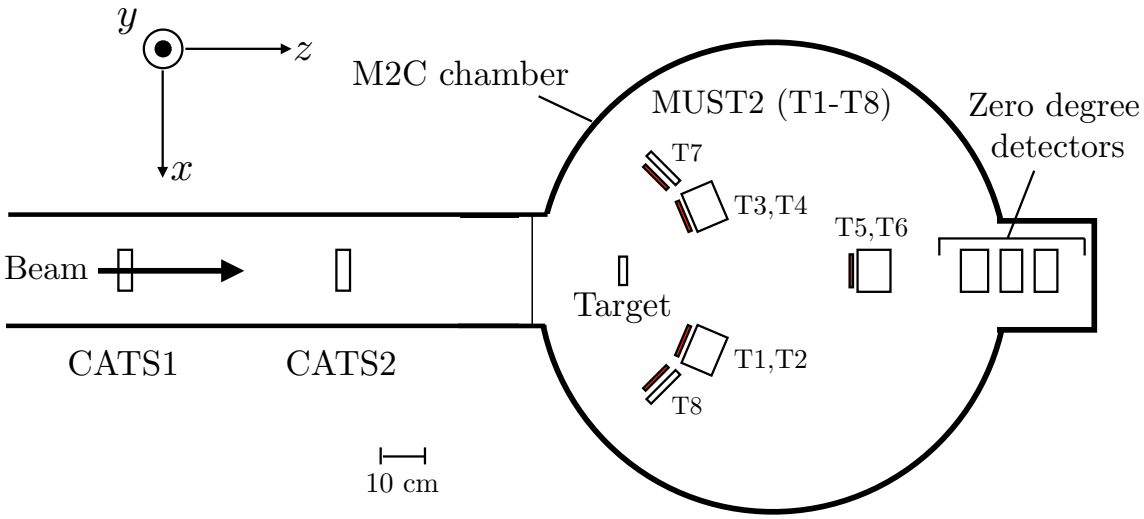

Fig. 2.4 Schematic setup of the present experiment.

to measure the hit positions and angles of the beam particles. We will call these detectors CATS1 and CATS2. The distance between CATS1 and the center of the liquid hydrogen target was 1118 mm while that between CATS2 and the target was 657 mm. The beam trajectories were reconstructed using the positions measured by CATSs. The TOF between RF signal of the cycrotron and CATSs were also measured for the beam PID.

CATS is a low pressure Multi-Wire Proportional Chamber (MWPC). It consists of two cells with common anode as shown in Fig. 2.5. The active area of the detector is 70 × 70 mm^2. The chamber anode is a plane of 71 gold plated tungsten wires which have a diameter of 10 μm and 1 mm spaced. The dead area from these wires are 1% of the active area. All the wires are connected in parallel and the operating positive voltage. The supplied HV in the present experiment was from 660 to 680 V. This anode plane is located between two segmented cathode planes at a distance of 3.2 mm. The 28 gold strips of each plane are evaporated with a thickness of 200 nm on a 1.5 μm thick Mylar foil. The cathode pitch is 2.54 mm and the inter strip width is 0.2 mm. Two additional 1.5-μm self supporting Mylar windows close the gas circulation volume, to avoid any deformation of the cathode and preserve the uniformity of the electric field. The small thickness of these four windows ensures the transparency even with a low energy secondary beam. The detector was filled with pure isobutan (C_4H_{10}) at a pressure of 8 mbar.

When the particle ionizes the gas, the created electrons are accelerated by an electric field applied between the anode and the cathode and acquire enough energy to induce the avalanche phenomenon. At low pressure, the avalanche phenomenon takes place throughout the migration of the electrons. Their fast drift reached the wires of the anode and this

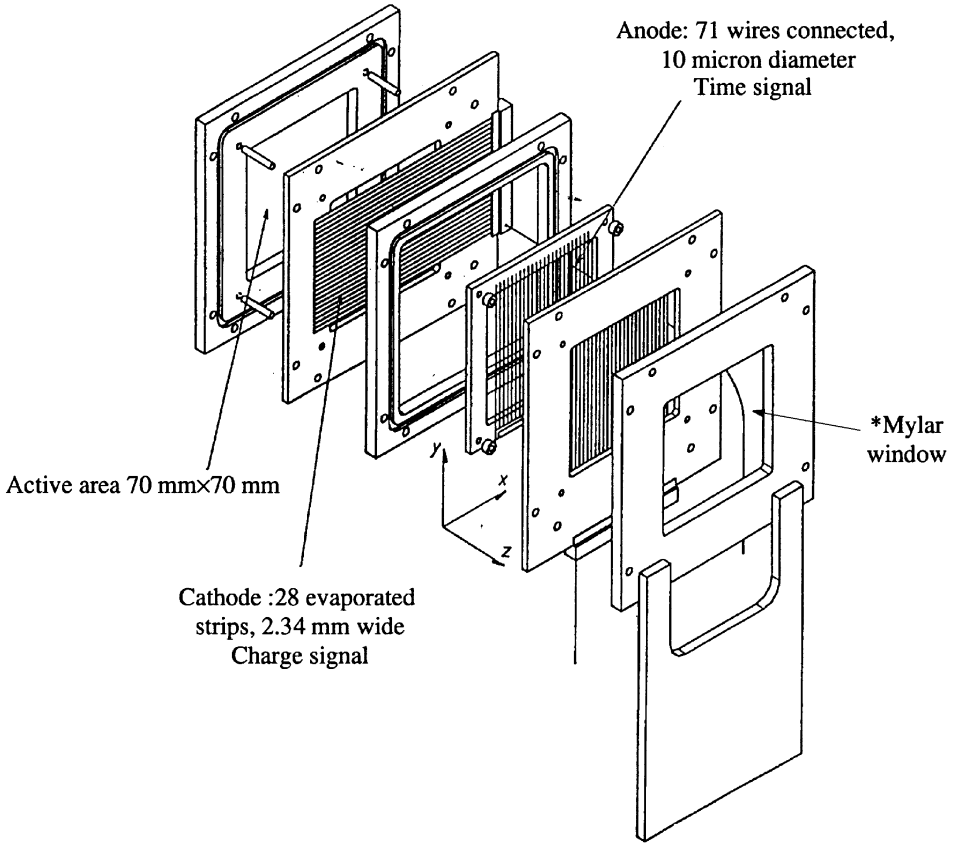

Fig. 2.5 Schematic view of a CATS. The figure is taken from [48].

signal is used as a time reference of the particle hit the CATS detector. In the vicinity of the wires, the electric field grows very rapidly and a second avalanche occurs. Given the short distance of the ions created, migrating towards the cathode, induce a signal on several tracks. Each of the 28 cathode strips has its own output and the charge of each signal is recorded. The distribution of the charge of the strips allows to deduce the position of the passage of the incident particle. The signals from the anode wires were used for TOF measurements while the charge distribution of the cathode strips was used to deduce the positions of the secondary beam particles. During the beam time, the cathode plane of each CATS was replaced once since the HV was not able to be supplied because of the radiation damage. The geometry measurement were performed just after the beam time.

2.4.3 Recoil particle detector; MUST2

Recoil particle detection from transfer reactions is required for the measurements via the missing mass spectroscopy. Particle identification and momentums measurements are needed. An array of eight MUST2 [49] telescopes was placed to detect the recoil particles.

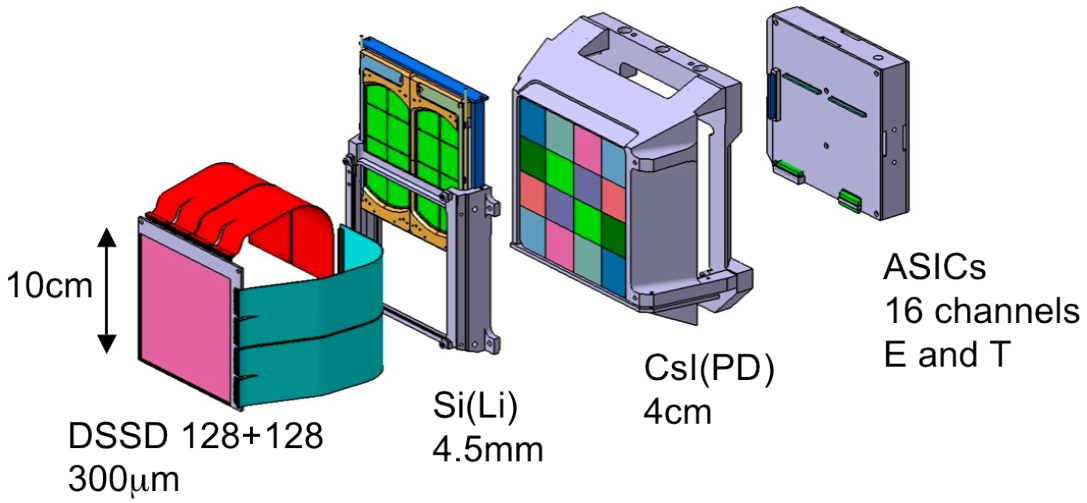

Fig. 2.6 Configuration of the MUST2 telescopes T5-T8.

Large acceptance and good energy and angle resolution of MUST2 allow us to deduce excitation spectra and angular distributions from transfer reactions. Not only the recoil particles but also light fragments such as protons and α particles were detected in the present experiment. This detector is designed for operation under a vacuum of the order of 10^{-6} mbar to prevent the recoil particles from reacting with air.

Figure 2.6 shows a schematic view of a MUST2 telescope. MUST2 has three layers of detectors, a double-sided silicon strip detector (DSSD), a lithium-drifted silicon detector (Si(Li)) and a talium doped CsI scintillation detector (CsI(Tl)). An electronic board, called MUFFEE, is assembled at the back of the telescope. MUFFEE drives the multiplex processing of the detector signals. Eighteen chips of Application Specific Integrated Circuit (ASIC) are also assembled on the board. The heat from the signal processing can not escape by air since these boards are put in the vacuum during the experiment. The temperature of the ASIC was kept about -2°C by a circulating cooling system for the stable operation.

Eight MUST2 telescopes were named T1 to T8 and placed as shown in Figs. 2.7. Geometrical acceptance of the array is also shown in Fig. 2.8. The positions of T1 to T4 were shifted about -85 mm from the standard position to cover the angle up to about 35°, which is the maximum angle of the (p, d) reaction. As shown in Fig. 2.8 (a), T1 to T4 covered the laboratory angle from 10 to 40°, which covered both of the (p, d) and (p, t) reactions as shown in Fig. 2.8 (b). To cover the most forward angle, T5 and T6 were placed at the downstream of T1 to T4. To prevent the unreacted beam particle from directly hitting these telescopes, the mechanical frame of T5 and T6 were made to change

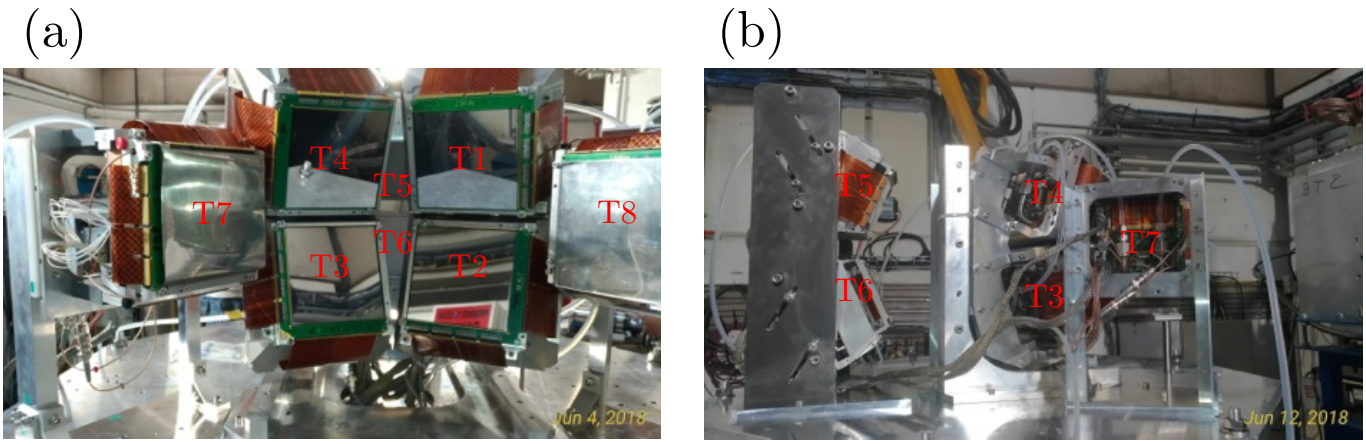

Fig. 2.7 Photographs of the configuration of the MUST2 telescopes. (a) A photo taken from the upstream of the beam line. T5 and T6 are partially covered by T1 to T4. (b) A photo taken from the side of the beam line.

distance between T5 and T6. Finally we set the distance of T5 and T6 60 mm, which covers from 3 to 10°. T7 and T8 were placed relatively large angle to detect elastic and inelastic events, which covers from 50 to 70°. Note that T7 and T8 were not used in the present analysis.

In the present experiment, six telescopes (T1 to T6) had DSSD and CsI(Tl) layers while two telescopes (T7 and T8) had DSSD and Si (Li) layers. DSSDs provide position, energy (ΔE) and time measurements for each particle. The second or third layer layer measures the remaining energy (E). The remaining energy were measured by Si(Li) or CsI(Tl). This allows identification of the particle in charge and in mass by $\Delta E - E$ method as well as the measurement of its total energy. Momentum of the particle are reconstructed from the total energy and the angle deduced by position measured by DSSD and a reaction point at the reaction target deduced by CATSs.

Detail of each layer is explained in the following.

DSSD

A DSSD is placed as a first layer of MUST2. It has an active area of about 300 μm thick and 98×98 mm^2. Each side of the detector is segmented in 128 strips with a 0.76 mm pitch. The thickness of the dead layer of the DSSD is about 0.5 μm. About 0.4 μm aluminum layers are evaporated as electrodes at the surface of the DSSD. The thickness of the SiO_2 layer, deposited on the silicon substrate and then doped at the strips to create the p and n junction, is of about 0.1 μm. Each strip is separated by an inter-strip of. The energy resolution is about 40 keV FWHM and time resolution is 250 ps FWHM with

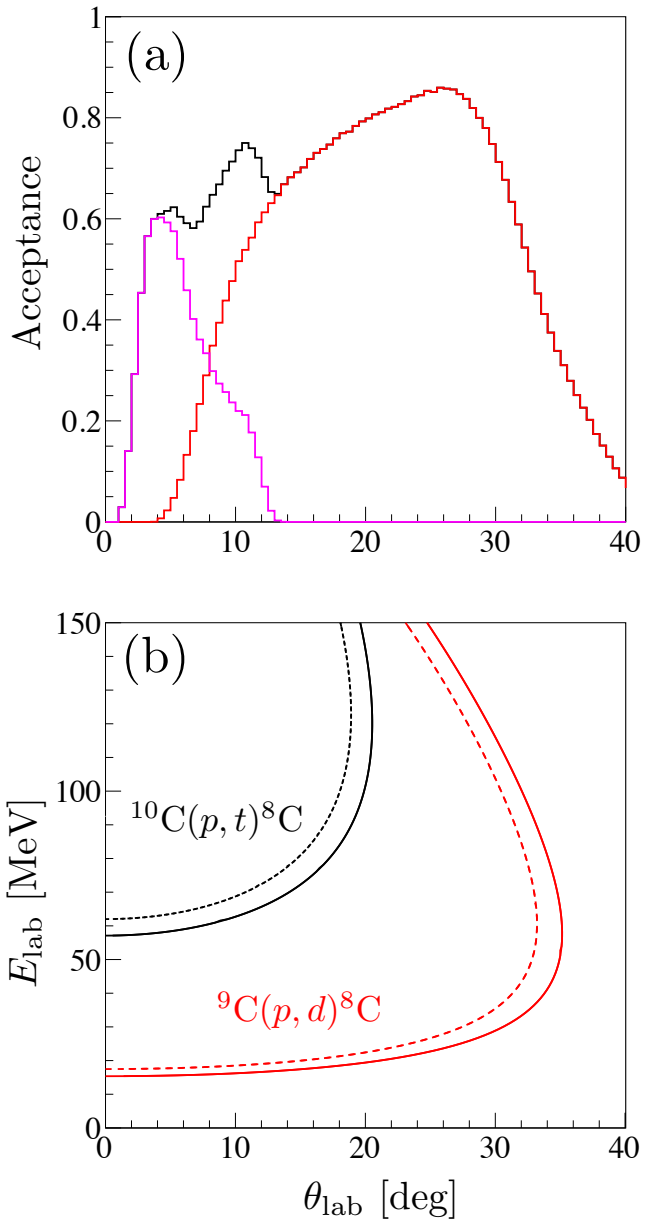

Fig. 2.8 (a) Geometrical acceptance of the MUST2 telescopes. The total acceptance of T1-T6 are shown by black. The acceptance of T1-T4 is shown by red while that of T5 and T6 is shown by magenta. (b) Kinematic curves of the transfer reactions. The curves for the ^{9}C$(p,d)^{8}$C reaction leading to the ground state is shown by red solid line while that leading to the 3.5 MeV excited state is shown by red dotted line. The curves for the ^{10}C$(p,t)^{8}$C is shown by black solid and dotted line.

5.5 MeV α source. The operating voltage during the beam time was from 60 to 80 V and the leak current was from 0.5 to 6.0 μA.The energy threshold was set to be about 0.5 MeV, which is as low as the energy deposit of 150-MeV deuteron in the DSSD.

Si(Li)
A Si(Li) was placed at 17 mm from the DSSD of T7 and T8. This detector is composed of two Si(Li)s, which are divided by 8 pads. It has an active area of about 4.5 mm thick and 100×50 mm^2. The geometrical coverage to a DSSD is about 65%. The energy resolution is about 130 keV FWHM with 5.5 MeV α source. The stopping power is not enough for the recoil particle from transfer reaction though the Si(Li) has better resolution than CsI(Tl).

CsI(Tl)
16 CsI(Tl) crystals placed were placed at 30 mm from the DSSD of T1 to T6. It has an active area of about 40 mm thick. The crystals are tapered from 122×122 mm^2 at the entrance to 160×160 mm^2 at the exit. The shape of the crystal at each position is different to meet the condition. To ensure a maximum light output collection, the side of each CsI crystal is surrounded with a 50-μm thick alminized Mylar foil. The front of each CsI crystal is also covered by with a thinner 3-μm thick alminized Mylar foil to minimize the dead layer of the detection. A Photodiode with 25.5×25.5 mm^2 is attached to the back side of each CsI crystal. The area of the back side which is not covered by the photodiode is covered by reflective material to prevent light leak. The energy resolution is about 330 keV FWHM with 5.5 MeV α source.

2.4.4 Zero degree detectors

To detect the beam-like fragment emitted in the zero degrees, a detector array composed of Drift Chambers, an Ionizing Chamber and a plastic scintillator was placed just downstream of the T5 and T6. These detector was placed for the recoil particles detection by MUST2 in coincidence with heavy fragments by the zero-degree detectors, which allowed us to have sensitivity for decay modes and clean excitation energy spectra. These detectors were optimized for the E755 experiment, in which nuclei with Z from 16 to 20 secondary beams were used.

Only the plastic scintillator was used to confirm the beam particle identification and not used to deduce the physical quantities.

Drift chambers
Four drift chambers were placed for the position and angle measurements of the beam-like fragments. Two are for the horizontal direction and the other two for the vertical direction.

Ionizing chamber
An ionizing chamber was placed just downstream of the drift chambers. The energy loss of the particles was measured and used for the fragment particle identification especially for Z.

Plastic scintillator
The plastic scintillator was placed at the end of the zero degree detectors. The particles in the zero degrees were stopped in this detector. The thickness was 20 mm. The light output was collected by a light guide attached the back of the plastic scintillator and gained by photo multiplier tube. The amplitude of the light output was recorded.

2.4.5 Position measurement

The positions of the detectors were measured before and after the beam time by a geometrical surveyor. The results of the geometrical survey are summarized in Tabs. 2.2 and 2.3.

Table 2.2 The result of the geometrical survey of the CATS detectors and the liquid hydrogen target.

	x [mm]	y [mm]	z [mm]
CATS1	-1.5	0.2	-1188.0
CATS2	-1.7	0.0	-678.5
Target	-3.3	-2.3	0.0

2.5 Data acquisition

The data were stored event by event using the standard data acquisition system at GANIL. The electric circuits for the detectors and the trigger conditions are described in this section.

Table 2.3 The result of the geometrical survey of the MUST2 telescopes.

	x [mm]	y [mm]	z [mm]		x [mm]	y [mm]	z [mm]
T1	13.48	103.89	213.34	T2	115.85	-11.15	206.14
T1	103.78	103.86	177.17	T2	104.28	-103.37	177.50
T1	115.43	11.81	206.33	T2	13.78	-103.10	213.40
T1	25.15	11.82	242.49	T2	25.35	-10.88	242.03
T3	-11.99	-103.71	212.91	T4	-113.70	11.02	206.13
T3	-102.20	-103.70	176.60	T4	-102.20	103.03	176.70
T3	-113.77	-11.43	205.09	T4	-11.87	103.30	212.80
T3	-23.52	-11.40	241.43	T4	-23.36	11.28	242.24
T5	-49.77	29.41	589.65	T6	48.39	-30.07	589.98
T5	-49.99	118.12	549.78	T6	48.30	-118.69	549.85
T5	47.28	118.51	550.09	T6	-48.99	-118.62	550.00
T5	47.51	29.80	589.95	T6	-48.93	-30.01	590.13
T7	-194.45	-48.63	86.03	T8	144.74	48.77	166.95
T7	-193.92	48.86	86.02	T8	199.10	49.10	86.36
T7	-139.72	48.53	166.65	T8	199.77	-48.22	86.39
T7	-140.23	-48.91	166.69	T8	145.39	-48.54	167.01

2.5.1 Electric circuit

MUST2

Totally 272-channels of charge signals from the DSSD and the CsI detector were generated by MUST2. These signals were processed by ASIC chips, called MATE, assembled on the MUFFEE board [50] equipped at the back of the telescope. The analog signals from the detectors were processed by preamplifiers. The amplified signal was divided into two. One was shaped by a fast-timing amplifier (FTA) with a 1-μs shaping time. The other was discriminated and the time difference with respect to the stop signal from CATS2 was converted into an analog pulse with a corresponding height by a time-to-amplitude converter (TAC).

All the generated analog signals were sent to a digitization module, called MUVI, after the signal processing on the MUFFEE board. The signals from up to four telescopes can be treated by a MUVI module. The signals were digitized by a 14-bit analog-to-digital converter (ADC). The dynamic range of about 16 kch was divided into two regions. The positive signal from the X strips is allocated to the region from 8 kch to 16 kch in increasing

order, while the negative signal from the Y strips, the CsI crystals and the TAC modules is from 8 kch to 0 kch in decreasing order. The dynamic ranges were typically set to be about 60 MeV for the DSSD and 200 MeV for the CsI scintillator, respectively.

The trigger of the respective telescopes (MT_i for the i-th telescope) were also created by the MUVI module when one of the DSSD strips had a sufficient signal amplitude over a threshold. In the present experiment, the threshold was set to be 0.5 MeV.

CATS

The charge signals from the cathode strips were processed by a pre-amplifier. The signals were then digitized by a 14-bit QDC module in the VXI crate. The signal from the anode strips was used for the generation of a logic pulse. The signal was shaped by a FTA module and a logic pulse was then generated by a constant-fraction discriminator (CFD). The logic pulses, $CATS_1$ and $CATS_2$ respectively, were used as the trigger source. The time difference with respect to the RF signal was measured for the the time-of-flight of the beam particle. The time difference was converted to an analog signal by a TAC module and digitized by a 14-bit ADC module.

Plastic

The charge signal from the photo multiplier tube of plastic scintillator was digitized by a 14-bit QDC module in the VXI crate. The signal was also discriminated by a CFD module and the generated logic pulse PLA was used as the trigger source.

2.5.2 Trigger

In the present experiment, the GANIL Master Trigger (GMT) module in the VXI standard was used for the triggering of the data acquisition. The GMT module has 16-channel trigger inputs. Three kinds of trigger sources were prepared. The single triggers from the MUST2 telescopes, MT_i (i=1-8), the triggers from CATS, $CATS_i$ (i=1, 2), and the triggers from the plastic scintillator, PLA, were put as the trigger inputs. The trigger of MT_i corresponds to the recoil particle detection by each MUST2 telescope to accumulate the physics data by the transfer reactions. The triggers of $CATS_i$ were prepared to count the number of the beam particles. The trigger of PLA was also prepared to estimate the transmission at the liquid hydrogen target. Using the down-scale module, $CATS_i$ and PLA were down-scaled by 3×10^4 and 1×10^4, respectively. The master trigger $Trig$ employed in the present experiment was defined by

$$Trig = MT \cup CATS \cup PLA \tag{2.1}$$

where MT is the logical sum of MT_i (i=1-8) and $CATS$ is the logical sum of $CATS_i$ (i=1, 2). The typical rate of $Trig$ was about 0.7 kHz and a mean dead time was 12%.

2.6 Data set

The data with three secondary beams, ^{9}C, ^{10}C and ^{12}C sets, was recorded. The data set is summarized in Table 2.4. Apart from the physics data with the liquid hydrogen target, the data without liquid hydrogen, called the empty target, was taken for the background subtraction.

Table 2.4 The summary of the data set.

Beam setting	Nuclei (purity)	Average intensity [pps]	duration [s]	target
1	^{10}C (100%)	1.2×10^5	1.1×10^5	LH_2
2	^{10}C (100%)	1.2×10^5	3.6×10^3	Empty
3	^{9}C (5%),^{8}B (10%), ^{7}Be (65%),^{6}Li (20%)	1.3×10^5	2.5×10^5	LH_2
4	^{9}C (5%),^{8}B (13%), ^{7}Be (65%),^{6}Li (20%)	1.3×10^5	4.8×10^4	Empty
5	^{12}C (100%)	1.1×10^5	5.7×10^4	LH_2

Chapter 3

Analysis

本章については、5 年以内に雑誌等で刊行予定のため、非公開。

Chapter 4

Results

本章については、5 年以内に雑誌等で刊行予定のため、非公開。

Chapter 5

Discussion

本章については、5 年以内に雑誌等で刊行予定のため、非公開。

Chapter 6

Conclusion and outlook

本章については、5 年以内に雑誌等で刊行予定のため、非公開。

Appendix A

Multi-wire proportional chamber CAVIAR

During the beam time, one tracking detector was placed in the LISE beam line. CAVIAR detector was placed to monitor the time of flight (TOF) and the horizontal position at a dispersive focal plane for $B\rho$ measurement of the beam particles at the upstream of the Wien filter. This detector was placed to prepare for the lower purity of the ^{9}C than expected. In that case, we had to open the first slit wider and the momentum range of the particle would be wider though the total intensity would become higher. Two problems could occur. One is for the secondary beam particle identification (PID). In this experiment, the PID was performed from TOF of RF-CATS detector as described later. With the wide range of momentum, the TOF values could overlap for the neighboring particle. In that case, the $B\rho$ deduced from the position measurement will help to perform the PID. The other is for the missing mass reconstruction. The energy resolution of the excitation energy from missing mass depends on the beam energy, though the effect is not so large in the usual case. In case the beam energy spreading will affect the excitation energy resolution, it could be also corrected by the $B\rho$ value.

A schematic view of the CAVIAR detector is shown in Fig. A.1 The sensitive area of this detector is 96 mm in the horizontal plane and 32 mm in the vertical plane, which covers the secondary beam sizes and maximum aperture of the slits in the dispersive plane. The CAVIAR detector is composed by 96 gold plated tungstain wires of 10 μm in diameter with 1 mm step between each of them. Two 1.5 μm thicknesses Aluminum Cathodes foils are placed 3.4 mm distance from the anode.

Detector is filled with Isobutene (C_4H_{10}) gas less than 50 mbar. Two Kapton windows of 8 μm thicknesses are used. They isolate the detector from beam line vacuum. The CAVIAR detecotr is a low interceptive detector for high energy beams.

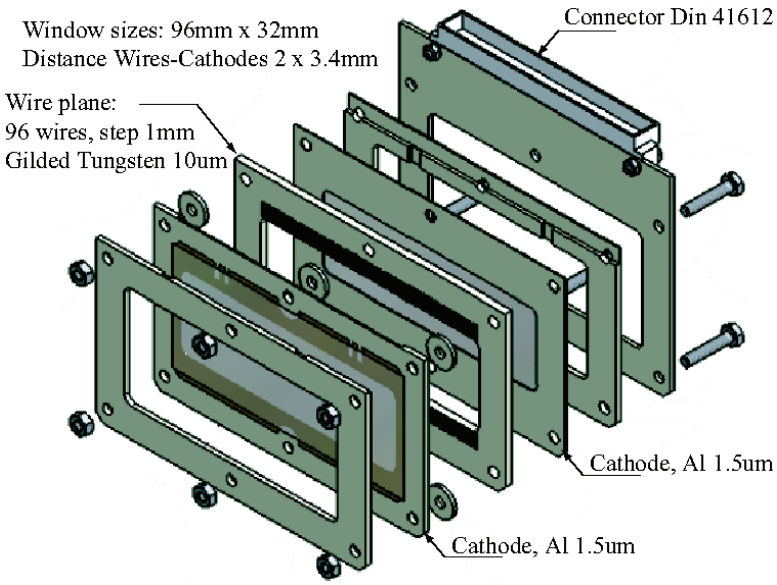

Fig. A.1 A schematic view of the CAVIAR.

In the present analysis, the data of CAVIAR was not used.

Appendix B

Operation of the target at the M2C chamber

本章については、5 年以内に雑誌等で刊行予定のため、非公開。

Appendix C

Correlation of the parameters of fit to excitation energy spectra

本章については、5 年以内に雑誌等で刊行予定のため、非公開。

Acknowledgments

First, I would like to express my sincere gratitude to my supervisor, Prof. Hiroyoshi Sakurai. The time I spent with him is not so long, but he always gave me invaluable comments and supported me when I needed it. I learned a lot from discussions with him, not only the nuclear physics.

I am truly grateful to Dr. Daisuke Suzuki, who is the spokesperson of the present E738 experiment at GANIL. He gave me an opportunity to join the experiment and a lot of invaluable advice throughout the processes; experiment, data analysis and discussion of the obtained results. I respect his uncompromising stance for experiments.

I would like to express my sincere appreciation to all the collaborators of the E738 experiment at GANIL. I am grateful to Dr. Marléne Assié, Dr. Didier Beaumel, Dr. Yorick Blumenfeld, Dr. Lucia Caceres, Dr. François De Oliveira, Dr. Franck Delaunay, Dr. Freddy Flavigny, Dr. Serge Franchoo, Dr. Julien Gibelin, Mr. Valérian Girardalcindor, Dr. Jacques Guillot, Dr. Faïrouz Hammache, Mr. Armel Kamenyero, Dr. Noritaka Kitamura, Dr. Valérie Lapoux, Dr. Antoine Lemasson, Mr. Louis Lalanne, Dr. Adrien Matta, Dr. Benoît Mauss, Dr. Pierre Morfouace, Dr. Megumi Niikura, Dr. Kamalou Omar, Dr. Hideaki Otsu, Dr. Julien Pancin, Dr. Thomas Roger, Mr. Takeshi Saito, Dr. Olivier Sorlin, Dr. Christelle Stodel, and Dr. Jean-Charles Thomas for their contributions. Especially, I appreciate the spokespersons of the LISE-MUST2 campaign experiments, Marléne, Olivier, Adrien and Dr. Gheorghe Iulian Stefan for their support in my life at GANIL for about half a year in total. I also thank the support of the group of Prof. Nigel Orr at LPC Caen for my stay at GANIL in 2017. I enjoyed the life in GANIL with the Ph.d. students Valérian, Louis and Armel. I would like to deeply thank the technical staffs of GANIL, particularity Mr. Vincent Morel, Mr. Sebastien Le Moal and Mr. Frank Pillon for the operation of the cryogenic target system at GANIL.

I would like to appreciate Dr. Takashi Abe for the discussion of the present results for a long time. I thank for the theoretical calculation of Prof. Noritaka Shimizu.

I would like to gratitude to all the members of the nuclear experiment (NEX) group at the University of Tokyo: Prof. Hiroyoshi Sakurai, Dr. Megumi Niikura, Dr. Nobuyuki Kobayashi, Dr. Ryo Taniuchi, Mr. Keishi Matsui, Dr. Satoru Momiyama, Mr. Takuya

Miyazaki, Mr. Takeshi Saito, Mr. Shunsuke Nagamine, Mr. Takamichi Aoki, Mr. Naoya Yoshida, Mr. Kei Kokubun, Dr. Kathrin Wimmer, Mr. Takuma Koiwai, Prof. Ryugo Hayano, Dr. Takatoshi Suzuki, Dr. Hideyuki Tatsuno, Mr. Yuya Fujiwara, Dr. Koichi Todoroki, Dr. Takahiro Nishi, Dr. Yoshiki Tanaka, Dr. Yohei Murakami, Mr. Hiroyuki Yamada, Dr. Yuni Watanabe, Mr. Hiroshi Horii and Mr. Takashi Ando. I am glad to spend a lot of time in the University of Tokyo with them.

I would like to express my thanks to Ms. Miwa Sugawara, Ms. Yuko Oshika, Ms. Yoshie Sayama and Ms. Kuniko Kono, the secretaries of the NEX group at the University of Tokyo. I also would like to thank to Ms. Emiko Isogai, Ms. Yu Naya and Ms. Asako Takahashi, the secretaries of RIKEN Nishina Center.

My special thanks go to Dr. Hideaki Otsu. I started my research in the graduate school with him and learned the basis. I could continue the present work with the basis.

I would like to express my gratitude to the thesis examiners, Prof. Susumu Shimoura, Prof. Hiroari Miyatake, Prof. Hiroaki Aihara, Prof. Osamu Morimatsu and Prof. Kyoichiro Ozawa for reviewing my thesis with many valuable comments.

Last but not least, I would like to thank my family for their continuous supports and encouragements.

Bibliography

[1] E. Rutherford, Philos. Mag. J. Sci. **21**, 669–688 (1911).

[2] C.F.v. Weizsäcker, Zeitschrift für Physik **96**, 431 (1935).

[3] O. Haxel, J.H.D. Jensen and H.E. Suess, Phys. Rev. **75**, 1766–1766 (1949).

[4] M.G. Mayer, Phys. Rev. **75**, 1969–1970 (1949).

[5] H. Horiuchi, K. Ikeda and K. Kat, Prog. Theor. Phys. Suppl. **192**, 1–238 (2012).

[6] W. v Oertzen, M. Freer and Y. Kanada-En' yo, Phys. Rep. **432**, 43 – 113 (2006).

[7] I. Tanihata, H. Savajols and R. Kanungo, Prog. Part. Nucl. Phys **68**, 215 – 313 (2013).

[8] F. Hoyle, The Astrophys. J. Suppl. Ser. **1**, 12 (1954).

[9] C. Cook *et al.*, Phys. Rev. **107**, 508 (1957).

[10] I. Tanihata *et al.*, Phys. Rev. Lett. **55**, 2676–2679 (1985).

[11] T. Kobayashi *et al.*, Phys. Rev. Lett. **60**, 2599–2602 (1988).

[12] A.B. Migdal, Sov. J. of Nucl. Phys. **16,**, 238 (1973).

[13] I. Tanihata, J. Phys. G: Nucl. Part. Phys **22**, 157–198 (1996).

[14] P. Navrátil *et al.*, Physica Scripta **91**, 053002 (2016).

[15] H. Kamada *et al.*, Phys. Rev. C **64**, 044001 (2001).

[16] B.S. Pudliner *et al.*, Phys. Rev. Lett. **74**, 4396–4399 (1995).

[17] M. Włoch *et al.*, Phys. Rev. Lett. **94**, 212501 (2005).

[18] P. Navrátil, J.P. Vary and B.R. Barrett, Phys. Rev. Lett. **84**, 5728–5731 (2000).

[19] R. Wiringa *et al.*, Phys. Rev. C **62**, 014001 (2000).

[20] R.G.H. Robertson *et al.*, Phys. Rev. Lett. **32**, 1207–1209 (1974).

[21] J. Cerny *et al.*, Phys. Rev. C **10**, 2654–2656 (1974).

[22] R.E. Tribble, R.A. Kenefick and R.L. Spross, Phys. Rev. C **13**, 50–54 (1976).

[23] R.G.H. Robertson *et al.*, Phys. Rev. C **13**, 1018–1023 (1976).

[24] R.J. Charity *et al.*, Phys. Rev. C **84**, 014320 (2011).

[25] T. Miyazaki, Master thesis (2015).

[26] A. Korsheninnikov *et al.*, Phys. Lett. B **316**, 38 – 44 (1993).

[27] H. Bohlen *et al.*, Prog. Part. Nucl. Phys. **42**, 17 – 26 (1999).

[28] V. Lapoux *et al.*, Nucl. Phys. A **722**, C49 – C54 (2003).

[29] M. Golovkov *et al.*, Phys. Lett. B **672**, 22 – 29 (2009).
[30] M. Holl *et al.*, *The 10th international conference on Direct Reactions with Exotic Beams* (2018).
[31] National nuclear data center.
[32] R.F. Casten, *Nuclear Structure from a Simple Perspective.*
[33] S. Quaglioni and P. Navrátil, Phys. Rev. Lett. **101**, 092501 (2008).
[34] G. Hagen, T. Papenbrock and M. Hjorth-Jensen, Phys. Rev. Lett. **104**, 182501 (2010).
[35] K.M. Nollett *et al.*, Phys. Rev. Lett. **99**, 022502 (2007).
[36] C. Romero-Redondo *et al.*, Phys. Rev. Lett. **117**, 222501 (2016).
[37] L.A. Kull, Phys. Rev. **163**, 1066–1073 (1967).
[38] N. Timofeyuk and R. Johnson, Prog. Part. Nucl. Phys. **111**, 103738 (2020).
[39] F.P. Brady *et al.*, Phys. Rev. C **16**, 31–41 (1977).
[40] G. JACOB and T.A.J. MARIS, Rev. Mod. Phys. **45**, 6–21 (1973).
[41] T. Yamada, M. Takahashi and K. Ikeda, Phys. Rev. C **53**, 752–764 (1996).
[42] D. Suzuki *et al.*, Phys. Rev. Lett. **103**, 152503 (2009).
[43] D. Suzuki, Eur. Phys. J. A **48**, 130 (2012).
[44] D. Suzuki *et al.*, Phys. Rev. C **93**, 024316 (2016).
[45] R. Anne *et al.*, Nucl. Instrum. and Meth. A **257**, 215 – 232 (1987).
[46] R. Anne and A.C. Mueller, Nucl. Instrum. and Meth. B **70**, 276 – 285 (1992).
[47] H. Ryuto *et al.*, Nucl. Instrum. and Meth. A **555**, 1 (2005).
[48] S. Ottini-Hustache *et al.*, Nucl. Instrum. and Meth. A **431**, 476 – 484 (1999).
[49] E. Pollacco *et al.*, Eur. Phys. J. A **Supplement 1**, 287 (2005).
[50] P. Baron *et al.* Ieee nuclear science symposium.
[51] O. Tarasov and D. Bazin, Nuclear Instruments and Methods in Physics Research Section B: Beam Interactions with Ma terials and Atoms **266**, 4657 – 4664 (2008).
[52] A. Wagner *et al.*, Nucl. Instr. and Meth. A **456**, 290 – 299 (2001).
[53] P. Descouvemont and D. Baye, Rep. Prog. Phys. **73**, 036301 (2010).
[54] N. Michel, Computer Physics Communications **176**, 232 – 249 (2007).
[55] Y. Ishizaki *et al.*, J. Phys. Soc. of Japan **20**, 2118–2128 (1965).
[56] P. Roos *et al.*, Nucl. Phys. A **255**, 187 – 203 (1975).
[57] J. Nelson, N. Chant and P. Fisher, Nucl. Phys. A **156**, 406 – 448 (1970).
[58] S. Cosper *et al.*, Phys. Lett. B **25**, 324 – 327 (1967).
[59] C.A. Pruneau, *Data Analysis Techniques for Physical Scientists.*
[60] A.A. Korsheninnikov *et al.*, Phys. Rev. Lett. **82**, 3581–3584 (1999).
[61] A.H. Wuosmaa *et al.*, Phys. Rev. C **72**, 061301 (2005).
[62] A.H. Wuosmaa *et al.*, Phys. Rev. C **78**, 041302 (2008).
[63] M.J. Balbes *et al.*, Phys. Rev. C **43**, 343–346 (1991).

[64] K.W. Brown *et al.*, Phys. Rev. C **95**, 044326 (2017).
[65] N. Shimizu, *Private communication.*
[66] S. Cohen and D. Kurath, Nuclear Physics **73**, 1 – 24 (1965).
[67] T. Teichmann and E.P. Wigner, Phys. Rev. **87**, 123–135 (1952).
[68] S. Funada, H. Kameyama and Y. Sakuragi, Nucl. Phys. A **575**, 93 – 117 (1994).
[69] K. Hagino and H. Sagawa, Phys. Rev. C **72**, 044321 (2005).
[70] G. Papadimitriou *et al.*, Phys. Rev. C **84**, 051304 (2011).
[71] Y. Jaganathen *et al.*, Phys. Rev. C **96**, 054316 (2017).
[72] K. Hagino, N. Takahashi and H. Sagawa, Phys. Rev. C **77**, 054317 (2008).
[73] F. Kobayashi and Y. Kanada-En'yo, Phys. Rev. C **88**, 034321 (2013).
[74] L.V. Grigorenko *et al.*, Phys. Rev. C **80**, 034602 (2009).
[75] T. Oishi, K. Hagino and H. Sagawa, Phys. Rev. C **90**, 034303 (2014).
[76] Y. Kikuchi *et al.*, Phys. Rev. C **88**, 021602 (2013).
[77] K. Hagino and H. Sagawa, Phys. Rev. C **89**, 014331 (2014).
[78] D. Wilkinson, *Isospin in nuclear physics.*
[79] P. Heiss and H. Hackenbroich, Nucl. Phys. A **162**, 530 – 540 (1971).
[80] K. Ikeda, N. Takigawa and H. Horiuchi, Prog. Theor. Phys. **40**, 277 (1968).
[81] S. Satsuka and W. Horiuchi, Phys. Rev. C **100**, 024334 (2019).
[82] T. Yamagata *et al.*, Phys. Rev. C **95**, 044307 (2017).
[83] S. Furusawa *et al.*, Astr. J. **774**, 78 (2013).
[84] S. Typel *et al.*, Phys. Rev. C **81**, 015803 (2010).
[85] M. Hempel *et al.*, Phys. Rev. C **84**, 055804 (2011).
[86] G. Röpke, Phys. Rev. C **79**, 014002 (2009).
[87] F. James, *Function Minization and ERROR Analysis Ver. 94.1.*